Modeling Pressure Fluctuations via Correlation Structure in a Gas–Solids Fluidized Bed

Zhen He and Weidong Zhang
Dept. of Optical and Scientific Instrument Engineering, Zhejiang University, Hangzhou, P.R. China

Keming He
Dept. of Physics, Hangzhou University, Hangzhou, P.R. China

Bochuang Chen
Dept. of Chemical Engineering, Zhejiang University, Hangzhou, P.R. China

The pressure fluctuations in fluidized beds contain useful information for indexing the quality of fluidization. However, the highly random and nonlinear signal is hard to investigate and far from being fully understood, which eventually hampers its industrial application. Many scholars have studied the causes of the pressure fluctuations (Fan et al., 1981, and references therein). Aside from the influence of the operating condition, Fan et al. (1981) demonstrated that the coalescence and motion of bubbles appear to be the major causes of the pressure fluctuations, while gas jetting, the formation of small bubbles above the distributor, and the raining of fluidized particles in the upper half of the beds also contribute to the pressure fluctuation. Roy et al.'s (1990) results showed that local pressure fluctuations appear to be characteristic of large fluctuations in other parts of the bed. The fractal feature was also explored in the gas–solids fluidized bed. Taking the long-term correlation property exhibited in the signal into account, Neogi et al. (1993) considered the signal as the product of a sine wave and fractional Gaussian noise. The multifractal character of the signal was also discussed by Zhong et al. (1996). Applying chaos theory to the analysis of pressure fluctuations in gas–solids fluidized beds has recently become popular, as it provides an interesting insight into the system's chaotic characteristics (Hay et al., 1995; Schouten et al., 1996).

In this article, we study the signal composition from its correlation structure. A great deal of evidence of the relatively slow decay of the autocorrelation function via time lag for the signal (for example, see Figure 8 in Fan et al., 1981; Figures 5–10 in Neogi et al., 1988; Figures 9–12 in Neogi et al., 1993) suggests that the inherent long-term correlation component exists in the time series. We think that this feature can be attributed to the intrinsic causality of bubble growth and motion, the endurance of the pressure fluctuations they cause, and the statistical similarity of the bubble phase in the bed at different times. Also, the nonstationarity of the signal was recently demonstrated by He et al. (1997). In order to model this part of the pressure fluctuations, fractional Brownian motion (FBM) introduced by Mandelbrot and Ness (1968) appears to be an appropriate candidate. It is a zero-mean, nonstationary Gaussian random process with statistical self-similarity. If one denotes FBM as $B_H(t)$, its covariance function

$$R_{B_H}(t,s) \sim |t|^{2H} + |s|^{2H} - |t-s|^{2H}, \tag{1}$$

where H is the self-similarity parameter. It is clear that $B_H(t)$ bears the infinite correlation property. The parameter H controls the "roughness" of FBM, which corresponds to the fractal dimension:

$$D = 2 - H. \tag{2}$$

The greater the parameter H, the more regular the FBM appears. In fact, one tends to search for periodicity in the signal for large H value. H also controls the shape of the average spectral density of FBM, defined as (Flandrin, 1989)

$$S(f) = \frac{C}{|f|^{\gamma}}, \tag{3}$$

where

$$\gamma = 2H + 1 \tag{4}$$

and C is a constant.

Correspondence concerning this article should be addressed to Z. He.
Address for Z. He: 12-1-402, Youyi Xincun, Songmuchang, Hangzhou, 310007, P.R. China.

On the other hand, the pressure fluctuations caused by the gas jetting at the distributor, formation of small bubbles near the distributor, and the turbulence of the fluidized particles exhibit the characteristics of "random noise," which has a wide range of spectrum content and holds a very short-term correlation attribute. Theoretically, we can regard this aspect of the pressure fluctuations as the superposition of numerous very small fluctuations caused by these minor factors (Pigford and Baron, 1965; Zhu et al., 1993). It is reasonable to suppose that each of these very small fluctuations obeys the same statistical distribution and is independent of the others. Thus, this part of the pressure fluctuations can be modeled as Gaussian white noise (GWN) $W(t)$, with the covariance function

$$R_w(t,s) = \sigma_w^2 \delta(t-s), \tag{5}$$

where the σ_w is the intensity parameter.

Since the physical sources of the two signal components are different and no apparent link exists between them, the two signal components can be assumed to be statistically independent. Furthermore, by taking the evidence of the probability density function provided by Fan et al. (1981), it is reasonable to regard the relation between the two components as additive. Thus, a practical model based on the correlation structure for the pressure fluctuation signal $X(t)$ is obtained by synthesizing the two parts discussed earlier.

$$X(t) = B_H(t) + W(t). \tag{6}$$

It now remains to effectively determine the self-similarity parameter H of FBM and the intensity parameter σ_w of GWN in the model. Fortunately, recently developed wavelet transform (Daubechies, 1988; Mallat, 1989b) makes such estimations possible.

The orthonormal wavelet transform (OWT) of a signal $X(t)$ is defined by

$$x(t) = \sum_{m=-\infty}^{+\infty} \sum_{n=-\infty}^{+\infty} d_n^m \psi_n^m(t)$$

$$d_n^m = \int_{-\infty}^{+\infty} x(t) \psi_n^m(t)\, dt, \tag{7}$$

where

$$\psi_n^m(t) = 2^{m/2} \psi(2^m t - n) \tag{8}$$

is the wavelet orthonormal basis obtained by the dilation and translation of a wavelet function $\psi(t)$ with good time-frequency localization, which can be constructed through multiresolution analysis. For a given scale m, the d_n^m extract information in the signal from resolution 2^m to resolution 2^{m+1} around time $2^{-m}n$. An efficient discrete-time implementation of the wavelet transform, called the pyramidal algorithm, can be found in Mallat (1989a).

The self-similarity and excellent time-frequency localization of the wavelet basis have made it a fascinating tool for studying FBM, which is inherently nonstationary and statistically self-similar (Mallat, 1989a; Wornell, 1990; Flandrin, 1992).

Applying OWT to both sides of Eq. 6, one can prove the following result (Wornell and Oppenheim, 1992):

$$\operatorname{Var} x_n^m = \sigma^2 \beta^{-m} + \sigma_w^2$$

$$\beta = 2^{2H+1}, \tag{9}$$

where x_n^m is the OWT coefficient for $X(t)$; $\operatorname{Var} x_n^m$, represents the variance of x_n^m at a given scale m; and σ^2 is a positive constant that is dependent on the choice of the wavelet function, the absolute labeling of the scales, and the constant C in Eq. 3. The clear and simple expression of H and σ^2 in Eq. 9 offers the possibility of estimating them effectively.

Actually, two favorable algorithms based on Eq. 9 have been developed to estimate the parameters (Wornell and Oppenheim, 1992; Kaplan and Kuo, 1993). Since Kaplan and Kuo (1993) have demonstrated that both algorithms can achieve very good estimates for longer data length (e.g., the length of the data equals 2048), Wornell and Oppenheim's algorithm has been adopted in this article.

A detailed proof and presentation of the algorithm can be found in Wornell and Oppenheim (1992). Here, we only summarize the main idea of the algorithm. The consistent iterative estimation algorithm based on the maximum likelihood method (ML). Although the main parameters of interest are H and σ_w, because of the dependence of σ on the implementation of the algorithm, the estimated parameter set is denoted $\theta = \{\beta, \sigma_w^2, \sigma^2\}$ in the algorithm. First, one calculates the OWT coefficients of the signal and obtains an estimate of the variance of the OWT coefficients at every fixed scale m. Then, using Eq. 9, one can carry out the ML estimates of the parameter set θ by differentiating the corresponding log-likelihood function $L(\theta)$ with respect to β, σ_w^2, σ^2, respectively, to get stationary-points equations. Utilizing an estimate-maximize (EM) algorithm, Wornell and Oppenheim (1992) derived an equivalent iterative algorithm to solve the stationary-points equations. The solutions of these equations are the expected parameters.

Experimental Section

The experiment was carried out in a fluidized bed 0.3 m in diameter and 3 m in height. The polyethylene (PE) particle was used as the fluidized particle, it had a density of 962 kg/m^3, and an average diameter of 523 μm. Its minimum fluidized-gas velocity u_{mf} is 0.157 m/s, and has a static-bed height of $H_s = 0.600$ m. The fluidizing fluid was air. The holes on the distributor were 2 mm in diameter and gave a fractional open area of 4%. Pressure probes were installed on the wall of the bed column at three different heights: 0.110 m, 0.370 m, and 0.610 m. The outside opening of each pressure probe was connected to one of the two input channels of a differential pressure transducer, which produces an output voltage proportional to the pressure difference between the two channels. The remaining channel was exposed to the atmosphere. The working capacity of the transducer was ± 5 kPa, and the relative accuracy error and the sensitivity of the whole measuring system were $\pm 0.5\%$ and 1 V/kPa, respectively. Since almost all frequency content is below 15 Hz, the sampling frequency was fixed at 50 Hz and its data length

was 2,048 every time. Daubechies' (1988) fourth-order finite-extent "maximally regular" wavelet basis with filter length equal to 8 was chosen to implement the algorithm. First, we calculated the OWT coefficients on seven scales and obtained the corresponding OWT coefficients' variance estimation on every scale m. Then, 6,000 iterations of the algorithm were successfully carried out to obtain a rather stable estimation for every data set. We repeated the experiments ten times for every fixed operating condition and obtained the mean value of the interesting parameters. The model was studied under different gas flow rates and static bed heights.

Results and Discussion

The changes of Hurst exponent H against u/u_{mf} at different probe distances above the distributor are shown in Figure 1. With all other operating conditions constant, this indicates that H increases following an increase in the superficial gas velocity u at the lower and middle portions of the bed, while tending to remain stable in the upper portion after a certain u a bit larger than the u_{mf}. Since the properties of the bubble phase mainly account for the pressure fluctuations in the gas–solids fluidized bed, we have to consider the change of the bubble phase via u to interpret the result. It is well known that both the coalescence and the splitting of bubbles exist in the gas–solids fluidized bed, but the probability of these two kinds of actions happening is not uniform throughout the bed. In the lower and middle portions of the bed, the coalescence process is more prevalent, while the splitting effect occurs less often, which is due to the relatively smaller diameter of the bubbles. Moreover, it is highly plausible that the bubble coalescence occurs in a probabilistic manner. Since the size

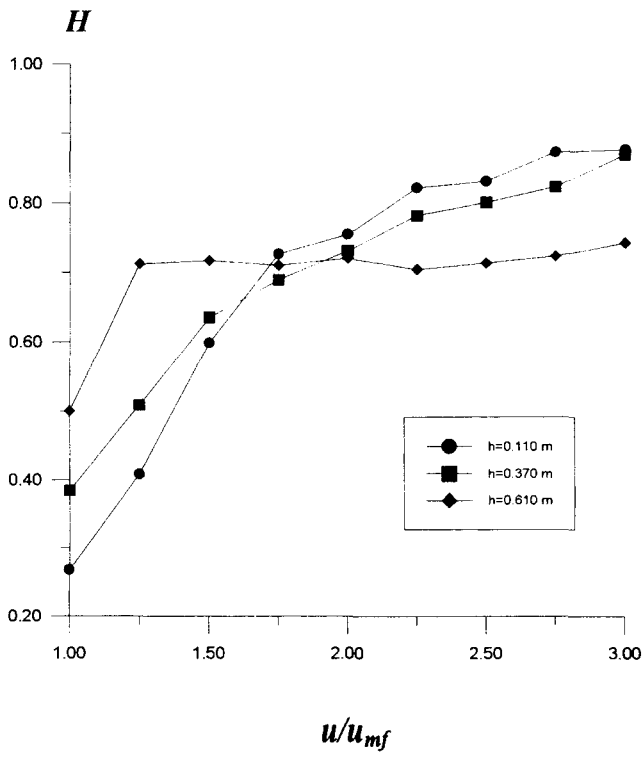

Figure 1. Change of Hurst exponent H against u/u_{mf}.

$H_s = 0.600$ m; $D_t = 0.300$ m; $u_{mf} = 0.157$ m/s.

of the bubbles at a fixed height only follows a probabilistic distribution, one of the sequences of the coalescence is the increase in the differences not only in the sizes but also in the rising velocities of the bubbles. Thus, intensification of the coalescence can destroy the uniformity of the flow pattern, which should weaken the persistence of the pressure-fluctuation signal generated under such conditions. In other words, a decrease in the coalescence frequency f_c can enhance the regularity of the pressure-fluctuation signal, which is reflected by increasing the Hurst exponent H. According to the Darton model (Darton et al., 1977), it is known that the bubble diameter

$$D_b \sim (u - u_{mf})^{2/5} h^{4/5} \tag{10}$$

at a distance h above the distributor and a superficial gas velocity u in the bed. Consequently, the coalescence frequency f_c follows (Masayuki and Akira, 1986):

$$f_c \sim \frac{(u - u_{mf})^{1.5}}{D_b^{4.25}}. \tag{11}$$

Thus,

$$f_c \sim (u - u_{mf})^{-0.2} h^{-3.4}. \tag{12}$$

From Eq. 12, we know that coalescence frequency f_c decreases with an increase in u. Moreover, following the increase in u, the bubbling frequency becomes more regular and has a smaller distribution range (Nelson et al., 1993), which further enhances the uniformity of the flow pattern in the bed. Thus, that H increases with an increase in u in the lower and middle portions of the bed can be understood. The trend of the H in the upper portion of the bed is different, as pointed out before. We thought it was better to take both the coalescence and splitting effects into account to get a reasonable explanation. From Eq. 10, we know that the diameter of bubbles increases when they float up. Although a decrease in the coalescence frequency causes the flow pattern in these areas to be more uniform, it is well known that bigger bubbles are more likely to split. Moreover, intensification of the particle turbulence to increase the superficial gas velocity u should also contribute to greater instability among the bubbles in the upper portion. Thus the splitting effect, which we think should increase the size distribution of the bubbles and undermine the uniformity of the hydrodynamics mechanism, is strengthened by the rising of u. We think that the interaction of the factors may account for the trend of the H in the upper portion. In fact, if one looks at Eqs. 10 and 12, it can be seen that h has a greater effect on the bubble diameter and coalescence frequency f_c than the gas velocity u does. We think this explains why the Hurst exponent H of the upper portion reaches a stable value steeply at a small u, while that of the middle or lower portion increases its value more slowly following an increase in u to reach a relatively stable value. (It is apparent that the rising rate of H tends to slow following the increase of u to approach a stable value.) This explanation is qualitatively form the physical background. We cannot find any literature from experimental results of the

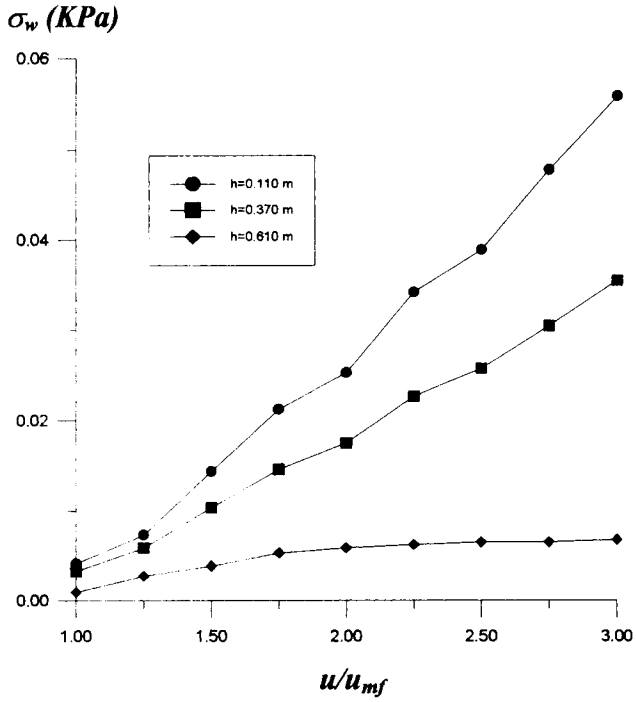

Figure 2. Change of intensity of Gaussian white noise σ_w against u/u_{mf}.

$H_s = 0.600$ m; $D_t = 0.300$ m; $u_{mf} = 0.157$ m/s.

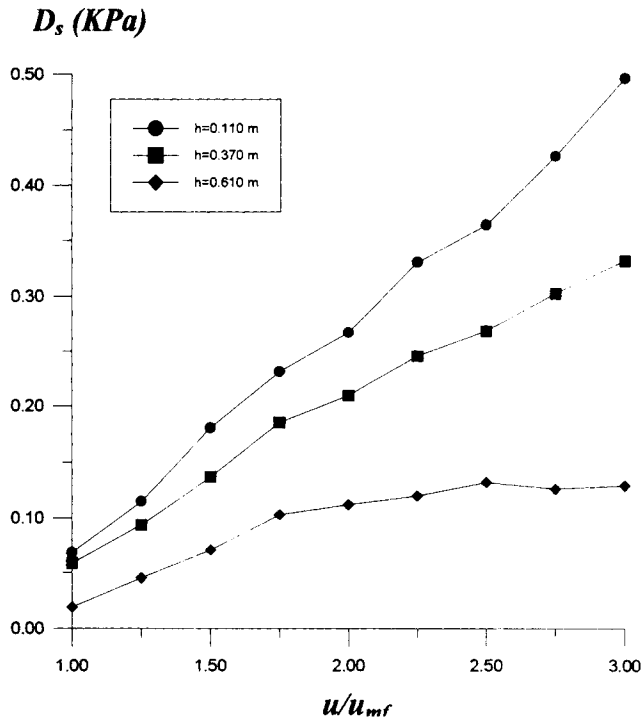

Figure 3. Change of signal standard deviation D_s against u/u_{mf}.

$H_s = 0.600$ m; $D_t = 0.300$ m; $u_{mf} = 0.157$ m/s.

change in bubble-size distribution in a 3-D gas–solids fluidized bed. This valuable task needs to be carried out. It is interesting to note that the FBM component in the pressure-fluctuation signal of the lower or middle portion exhibits the negatively correlated (antipersistent) feature $H < 0.5$ for lower u, but becomes positively correlated $H > 0.5$ after a certain value of u. A value of u exists that is dependent on h when the FBM component in the signal can be regarded as common Brownian motion with $H = 0.5$, which is an independent increment process. The physical meaning of this point needs to be explored further. In our case, this u is about $1.25u_{mf}$ for $h = 0.110$ m and $1.35u_{mf}$ for $h = 0.370$ m. Figure 1 also tells us that there seems to be no similar relation between H and h. At lower u, the H of the upper portion is larger than that of the lower portion, while the trend is reversed after a certain u. We thought this relation might also be interpreted by considering the effects of the coalescence and splitting of bubbles on the bubble-size distribution at different stages.

Figure 2 presents a variation of the GWN intensity parameter σ_w with u/u_{mf}. It is interesting to determine what content proportion the GWN component occupies in the signal as a whole. Since the standard deviation D_s of the signal can be considered as a measure of the intensity of the pressure fluctuation and bears the same dimension as σ_w, we define the parameter p_n to measure the content proportion of the GWN in the signal:

$$p_n = \frac{\sigma_w}{D_s} \cdot 100\% \tag{13}$$

The changes of D_s and p_n against u/u_{mf} are shown in Figures 3 and 4, respectively. As expected, D_s increases with u because the bubble size becomes larger as u increases (Fan et al., 1981). Since we are most interested in the white noise, we focus on Figures 2 and 4. Obviously, the σ_w of the lower portion of the bed increases rapidly when u goes up. This

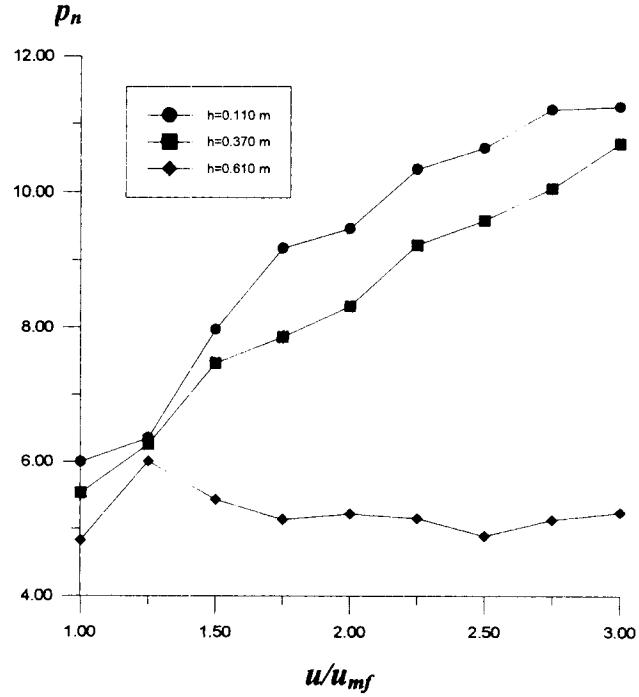

Figure 4. Change of parameter p_n against u/u_{mf}.

$H_s = 0.600$ m; $D_t = 0.300$ m; $u_{mf} = 0.157$ m/s.

trend is in accordance with the intensification of the jetting and formation of the small bubbles just above the distributor following an increase in u. The σ_w of the middle portion of the bed also increases with an increase of u, although the rate of increase is not as fast as that of the lower portion. The σ_w of the upper portion is rather insensitive to the change in u, and remains almost constant. The GWN in the upper portion may be induced mainly by the continuous raining of the fluidized particle on the bed surface (Fan et al., 1981). We can infer the following conclusions from the preceding results:

1. The jetting just above the distributor and the formation of small bubbles near the distributor are important sources, although they may not be the only ones, of the GWN component in the pressure-fluctuation signal.
2. The GWN caused by these sources is transmitted upward and gradually reduced by the increase in h.

The change in p_n in Figure 4 also confirms these conclusions. The direction of the change in p_n by u is consistent with that of σ_w. As indicated in Figure 4, the white-noise content proportion is within the range of $4.5 \sim 11.5\%$. Our results thus provide quantitative evidence of the statement: the small pressure fluctuations, which we think can be presented as GWN, are superimposed on the major fluctuations that we think can be characterized by FBM.

The effect of the static bed height H_s on H is presented in Figure 5. It indicates that H at $h = 0.110$ m is insensitive to the change in H_s; H at $h = 0.370$ m increases and moves toward a stable value with the increase in H_s; H at $h = 0.610$ m increases slightly following the increase in H_s. The interpretation needs further study.

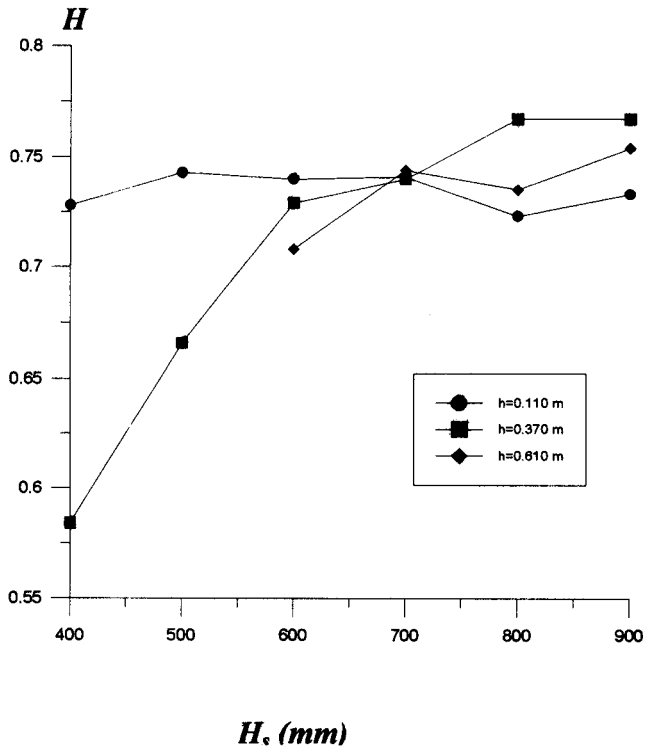

Figure 5. Change of Hurst exponent H against static bed height H_s.
$D_t = 0.300$ m; $u = 0.315$ m/s.

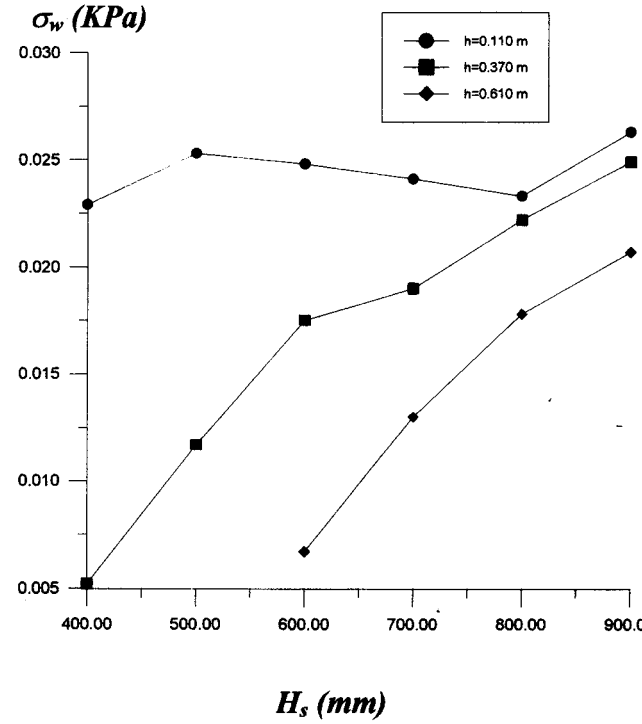

Figure 6. Change of intensity of Gaussian white noise σ_w against static bed height H_s.
$D_t = 0.300$ m; $u = 0.315$ m/s.

The tendency of σ_w against H_s is shown in Figure 6. The figure also shows that the greater the h, the smaller the value of σ_w, which has been explained earlier. It appears that H_s hasn't much effect on the σ_w of the lower portion. That may be because H_s has no significant function on the jetting and formation of small bubbles. The middle and upper portions seem to be subject to an increase in H_s. The higher the H_s, the greater the σ_w. We speculated that H_s might have some effect on the upward transmission of the GWN. The changes in D_s and p_n against H_s are described in Figures 7 and 8, respectively. It is apparent that D_s is intensified by an increase in H_s at a fixed h, while there seems to be no similar law to express D_s at different h if one takes H_s as a parameter. Figure 8 indicates that p_n decreases with an increase in H_s at the lower portion, while that of the middle portion appears to be irrelevant to H_s. After a certain value (in our case, it is between 0.600 and about 0.700 m), the p_n of the upper portion also expresses its independence of H_s. Taking Figures 6 and 7 into account jointly, this suggests that the entire FBM is intensified in the lower portion of the bed, while the intensity of each of the two components grows equally after a certain H_s for the middle portion and for the upper portion as H_s rises.

To demonstrate the satisfactory statistical reproducibility of the parameters, we list in Table 1 the results of ten estimates carried out under the same operating conditions, along with their mean, standard deviation, and relative standard deviation. As can be seen, both H and σ_w show excellent stability.

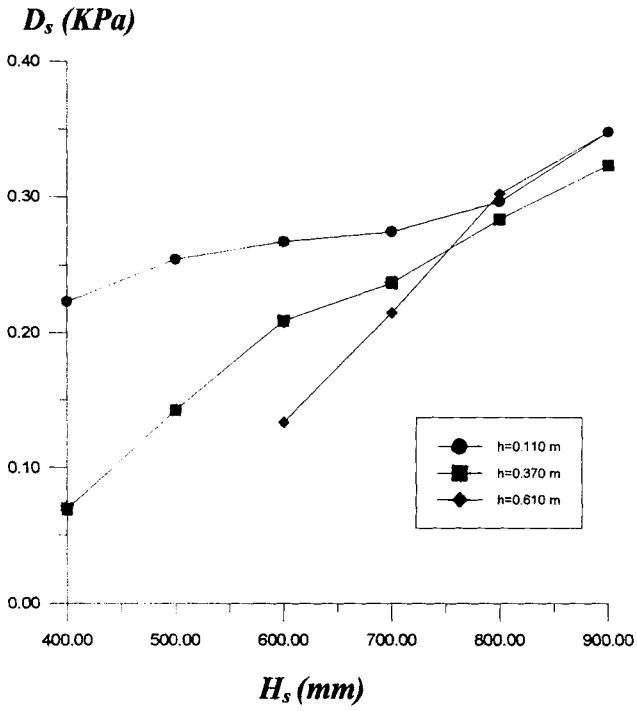

Figure 7. Change of signal standard deviation D_s against static bed height H_s.

D_t = 0.300 m; u = 0.315 m/s.

Conclusions

In this article, we have demonstrated that the pressure fluctuations in a gas–solids fluidized bed can be decomposed into the addition of FBM and GWN. A robust algorithm based on orthonormal wavelet transform was successfully applied to determine the self-similar parameter H of FBM and the intensity parameter σ_w of GWN in the model. The statistical reproducibility of the estimates is satisfactory. The H and σ_w were studied under different gas flow rates and static-bed heights. Consequently, we obtained the content proportion of the GWN p_n in the signal. Quantitative evidence was provided to draw the following conclusions: the jetting and the formation of the small bubbles near the distributor are important GWN sources of the pressure-fluctuation signal, although they may not be the only ones; the GWN caused by such origins is transmitted upward and reduced gradually by the increase in h; and GWN is superimposed on the largest pressure fluctuation that can be represented by FBM.

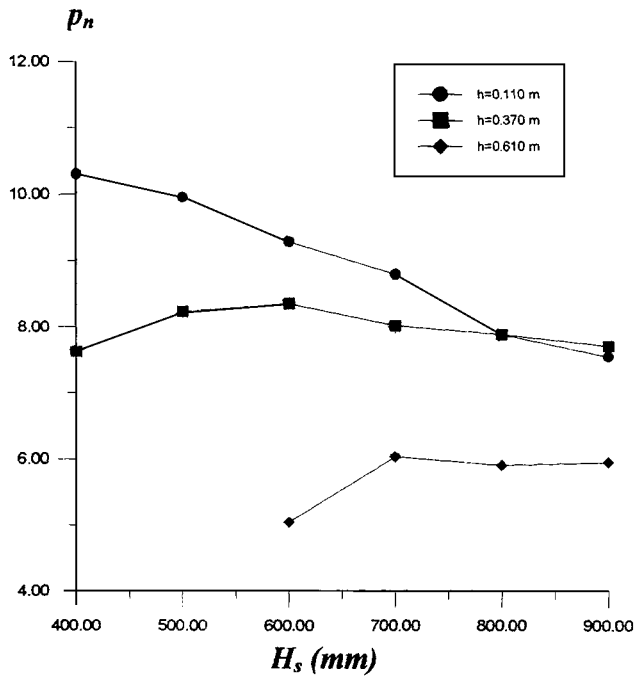

Figure 8. Change of parameter p_n against static bed height H_s.

D_t = 0.300 m; u = 0.315 m/s.

Table 1. Estimated Stability of H and σ_w for Experiments under Identical Operating Conditions*

Exp. No.	H	σ_w (kPa)
1	0.749	0.0188
2	0.729	0.0168
3	0.697	0.0171
4	0.742	0.0170
5	0.740	0.0177
6	0.725	0.0176
7	0.703	0.0164
8	0.726	0.0178
9	0.739	0.0163
10	0.765	0.0185

H:
Mean value = 0.732
Standard deviation = 0.0194
Relative standard deviation = 2.65%

σ_w (kPA):
Mean value = 0.0174
Standard deviation = 0.000792
Relative standard deviation = 4.55%

*u = 0.315 m/s; H_s = 0.600 m; h = 0.370 m.

Acknowledgment

We are deeply indebted to Professor George Stephanopoulos, who provided us with his research papers, and to Professor Gangtang Chen, whose discerning comments improved the readability of the article.

Notation

d_n^m = orthonormal wavelet transform coefficients
D_t = bed diameter
$R_{B_H}(t, s)$ = autocorrelation function of $B_H(t)$ at time t and s
γ = exponent of FBM average spectrum density

Literature Cited

Darton, R. C., R. D. Lanauze, J. F. Davidson, and D. Harrison, "Bubble Growth Due to Coalescence in Fluidized Beds," *Trans. Inst. Chem. Eng.*, **55**(2), 74 (1977).

Daubechies, I., "Orthonormal Bases of Compactly Supported Wavelets," *Commun. Pure Appl. Math.*, **41**, 909 (1988).

Fan, L. T., T. H. S. Hiraoka, and W. P. Walawender, "Pressure Fluctuations in a Fluidized Bed," *AIChE J.*, **27**, 388 (1981).

Flandrin, P., "On the Spectrum of Fractional Brownian Motions," *IEEE Trans. Inform. Theory*, **IT-35**, 1 (1989).

Flandrin, P., "Wavelet Analysis and Synthesis of Fractional Brownian Motion," *IEEE Trans. Inform. Theory*, **IT-38**, 2 (1992).

Hay, J. M., B. H. Nelson, C. L. Briens, and M. A. Bergouguou, "The Calculation of the Characteristics of a Chaotic Attractor in a Gas-Solid Fluidized Bed," *Chem. Eng. Sci.*, **50**(3), 373 (1995).

He, Z., D. Zhang, B. Chen, and W. Zhang, "Pressure Fluctuation Analysis of a Gas–Solids Fluidized Bed Using the Wigner Distribution," *AIChE J.*, **43**(2), 345 (Feb., 1997).

Kaplan, L. M., and J. C.-C. Kuo, "Fractal Estimation from Noisy Data via Discrete Fractional Gaussian Noise (DFGN) and the Haar Basis," *IEEE Trans. Signal Processing*, **ST-41**, 12 (1993).

Mallat, S. G., "A Theory for Multiresolution Signal Decomposition: The Wavelet Representation," *IEEE Trans. Pattern Anal. Mach. Intell.*, **PAMI-11**, 674 (1989a).

Mallat, S. G., "Multiresolution Approximations and Wavelet Orthonormal Bases of $L^2(R)$," *Trans. Amer. Math. Soc.*, **315**(1), 69 (1989b).

Mandelbrot, B. B., and V. W. J. Ness, "Fractional Brownian Motions, Fractional Noise, and Application," *SIAM Rev.*, **10**, 422 (1968).

Masayuki, H., and N. Akira, "A Generalized Bubble Diameter Correlation for Gas-solids Fluidized Beds," *AIChE J.*, **33**, 1865 (1986).

Nelson, B. H., C. L. Briens, and M. A. Bergougnou, "Pressure Fluctuations at Individual Grid Holes of a Gas-Solids Fluidized Bed," *Powder Technol.*, **77**, 95 (1993).

Neogi, D., L. T. Fan, N. Yutani, R. Nassar, and W. P. Walawender, "Effect of Superficial Velocity on Pressure Fluctuations in a Gas-solids Fluidized Bed: A Stochastic Analysis," *Appl. Stochastic Models Data Anal.*, **4**, 13 (1988).

Neogi, D., R. Nassar, and L. T. Fan, "Fractional Brownian Motion Modeling of Pressure Fluctuations in Multiphase Flow Systems," *Appl. Stochastic Models Data Anal.*, **9**, 19 (1993).

Pigford, R. L., and T. Baron, "Hydrodynamic Stability of a Fluidized Bed," *Ind. Eng. Chem. Fundam.*, **4**, 81 (1965).

Roy, R., J. F. Davidson, and V. G. Tuponogov, "The Velocity of Sound in Fluidized Beds," *Chem. Eng. Sci.*, **45**(11), 3233 (1990).

Schouten, J. C., M. L. M. Vander Stappen, and C. M. Vanden Bleek, "Scale-up of Chaotic Fluidized Bed Hydrodynamics," *Chem. Eng. Sci.*, **51**(10), 1991 (1996).

Wornell, G. W., "A Karhunen-Loeve-like Expansion for $1/f$ Processes via Wavelets," *IEEE Trans. Inform. Theory*, **IT-36**(4), 859 (1990).

Wornell, G. W., and A. V. Oppenheim, "Estimation of Fractal Signal Form Noisy Measurements Using Wavelets," *IEEE Trans. Signal Processing*, **SP-40**(3), 611 (1992).

Zhong, H., B. R. Bakshi, P. Jiang, and L. S. Fan, "Multifractal Characterization of Flow in Circulating Fluidized Beds," *Chem. Eng. J.*, in press (1996).

Zhu, J., H. Yu, and Y. Shi, "Study on Dynamics of Pressure Fluctuation for Slugging Fluidized Bed (II), Simulation and Experiment," *J. Chem. Ind. Eng.* (China), **44**, 4 (1993).

Manuscript received July 25, 1996, and revision received Feb. 7, 1997.